Original Article

Journal of Intelligent Material Systems and Structures

Journal of Intelligent Material Systems and Structures
2018, Vol. 29(4) 514–529

DOI: 10.1177/1045389X17711788
journals.sagepub.com/home/jim
SAGE

Investigation of direct current power delivery from nonlinear vibration energy harvesters under combined harmonic and stochastic excitations

Quanqi Dai and Ryan L Harne

Abstract

Leveraging smooth nonlinearities in vibration energy harvesters has been shown to improve the potential for kinetic energy capture from the environment as a transduced, alternating flow of electrical current. While researchers have closely examined the direct current power delivery performance of linear energy harvesters, there is a clear need to quantify the direct current power provided by nonlinear harvester platforms, in particular those platforms having bistable nonlinearities that are shown to have advantages over other smooth nonlinearities. In addition, because real world excitations are neither purely harmonic nor purely stochastic, the influences of an arbitrary combination of such excitation mechanisms on power delivery must be uncovered. To bring needed light to these roles and opportunities for nonlinear energy harvesters to provide direct current electrical power for numerous applications, this research formulates a new analytical approach to characterize simultaneous harmonic and stochastic mechanical and electrical responses of nonlinear harvester platforms subjected to realistic base excitation. Based on the outcomes of analytical, numerical, and experimental studies, it is found that additive stochastic excitation may result in direct current power enhancement via perturbation from a low amplitude state particularly at low frequencies or reduce the direct current power by preventing persistent snap-through response often at higher frequencies. When the noise standard deviation is greater than the harmonic amplitude by approximately two times, the advantages to direct current power generation are more often realized.

Keywords

Energy harvesting, nonlinear dynamics, direct current power

Introduction

Traditionally, the maintenance of engineered infrastructures is undertaken according to a scheduled basis, which is ineffective in the long-term due to accumulated expense and the serious potential for unintended failures (Randall, 2011). Condition-based structural health monitoring has risen as a promising alternative whereby the health of the infrastructures is assessed in real-time through a network of sensor nodes (Randall, 2011). Such sensors individually demand from around 100 μW to about 100 mW of direct current (DC) power supply, based on the function involved (Anon, 2015; Baert et al., 2006; Roundy et al., 2003). Because many of the sensors are placed so as to monitor the structural vibration levels as dynamic health indicators, kinetic energy is available to the sensor nodes. Thus, harvesting the kinetic energy using electromechanical oscillators collocated with the sensors has emerged as a way to realize self-sufficient structural health monitoring systems (Erturk and Inman, 2011b; Priya and Inman, 2009). In order to effectively harvest the kinetic energy from the structural oscillation, the vibration energy harvester must be sensitive to the ambient energy forms, because conventional electromechanical transduction mechanisms produce current flow in proportion to displacement or velocity of the mechanical response (Erturk and Inman, 2011b; Priya and Inman, 2009). Numerous researchers have found that the smooth nonlinearities of monostable and bistable

Department of Mechanical and Aerospace Engineering, The Ohio State University, Columbus, OH, USA

Corresponding author:
Ryan L Harne, Department of Mechanical and Aerospace Engineering, The Ohio State University, Columbus, OH 43210, USA.
Email: harne.3@osu.edu

Duffing oscillators may lead to broader spectral sensitivities to ambient vibrations than linear resonators, which has motivated considerable research attention to scrutinize the opportunities (Leadenham and Erturk, 2015; Mann and Sims, 2009; Masana and Daqaq, 2011a, 2011b; Tang et al., 2010).

The non-resonant nature of snap-through dynamics of bistable energy harvesters is a particularly advantageous feature for transduction, since the unique, large amplitude motions may be tuned and triggered with relatively low level input vibrations across a broad range of frequencies (Cottone et al., 2009; Daqaq, 2011; Erturk et al., 2009; Harne and Wang, 2014b, 2017; Stanton et al., 2010; Virgin, 2000). Despite the strong nonlinearity involved which challenges many theoretical tools, several research teams have studied base excited bistable energy harvesters coupled with resistive electrical circuits through rigorous analytical methods to assess alternating current (AC) power delivery opportunities. For instance, Stanton et al. (2012), Panyam et al. (2014), Daqaq (2011), and Harne and Wang (2014b) have leveraged various theoretical approaches to explicitly predict the AC power generation from bistable vibration energy harvesters when subject to either harmonic or stochastic base excitations. Despite the value of such insights, in order to supply useful power for structural monitoring sensor nodes, DC power must be delivered from the harvester. Thus, a rectifier circuit is needed to interface between the oscillatory electromechanical response and the electrical load. Rectifier circuits are dynamic systems, are nonlinear, and coupled to the dynamic response of the harvester itself, thus demanding special attention in model approaches (Liang and Liao, 2012; Shu and Lien, 2006a). Researchers have found that active synchronized switch harvesting on inductor circuits (Guyomar et al., 2005; Liang and Liao, 2012; Shu et al., 2007) and synchronized electric charge extraction circuits (Badel and Lefeuvre, 2016; Lefeuvre et al., 2005; Wu et al., 2012) enable promising DC power delivery for linear vibration energy harvesters under harmonic excitations. Comparatively, the simple and passive standard diode bridge rectifier provides an effective DC power delivery from linear and nonlinear vibration energy harvesters (Elvin, 2014; Pasharavesh et al., 2017; Shu and Lien, 2006b; Sodano et al., 2005) without unfavorable loss of power resulting from active synchronization. For instance, Shu and Lien (2006b) have shown that the electromechanical coupling coefficient is strongly influential on the mechanical-to-electrical energy conversion efficiency of linear energy harvesters interfaced with diode bridge rectifiers, which emphasizes the importance of comprehensively investigating the roles of practical rectifying circuits in contrast to AC resistive circuit counterparts. Yet, despite the significance of this knowledge, the insights are relevant only for linear vibration energy harvesters, while the analytical methodologies are not directly extensible to the numerous cases in which energy harvesters possess nonlinearities for performance enhancement.

Yet, considering the broad range of knowledge revealed by the studies surveyed above, such insights pertain only to the responses of energy harvesters when subjected to pure harmonic or pure stochastic excitations. In fact, numerous environments in which energy harvesters will be deployed alongside structural monitoring sensors do not exhibit such simple purely harmonic or stochastic excitation spectra. Instead, real world excitations contain a combination of noise and periodic contributions, which is inevitable based on the fact that the monitored structures oscillate in primary modes but are themselves acted upon by random excitations such as tire–road interaction or footfalls (Green et al., 2013; Turner and Pretlove, 1988; Zuo and Zhang, 2013). There is a clear lack of investigations on energy harvester electrodynamic responses that result from excitation conditions more closely representative of realistic vibrations. Although the dynamic sensitivities of weakly nonlinear oscillators have been examined under such conditions (Anh and Hieu, 2012; Bulsara et al., 1982; Nayfeh and Serhan, 1990), and a recent analysis has been presented to explore the purely mechanical responses of post-buckled structures to combined harmonic and stochastic perturbations (Harne and Dai, 2017), no such analysis exists to characterize the electromechanical responses and DC power delivery of nonlinear vibration energy harvesters subjected to arbitrary combinations of harmonic and stochastic base accelerations.

Motivated to close this fundamental knowledge gap, this research undertakes comprehensive efforts to characterize the DC power delivery from nonlinear vibration energy harvesters subjected to a combination of harmonic and stochastic excitation. Due to the strategic advantages of bistable nonlinearities, attention is directed to bistable energy harvesters, although the model and analytical methods presented pertain to the broader class of smooth, stiffness-based nonlinearities. The comprehensive efforts undertaken here notably include a new analytical procedure that facilitates direct prediction of the structural dynamics and electrical responses (including DC power), in parallel with a track of numerical simulation for verification and experiments for validation of the theoretical approach. The following sections first introduce the nonlinear bistable vibration energy harvester platform examined and describe the corresponding analytical framework established to investigate the platform. Then, a complement of analytical, numerical, and experimental results are presented to uncover the influences of the combined excitation form and electrical circuit parameters on the DC power delivery. A summary of primary conclusions and directions for future research are provided in the final section.

Nonlinear vibration energy harvester modeling

Energy harvester platform

This section introduces the experimental platform around which the model formulation is established, while further modeling details and analytical procedures are given in section "Governing equations," "Approximate analytical solution to governing equations," "Harmonic electromechanical dynamics," "Stochastic electromechanical dynamics," and "Combined harmonic and stochastic response of the nonlinear energy harvester." In this study, the energy harvester under consideration employs a pair of attractive magnets that act on a cantilevered piezoelectric energy harvester. The positioning of the magnets with respect to the ferromagnetic cantilever tip tailors the type and strength of the nonlinearity (Erturk and Inman, 2011a; Feeny and Yuan, 2001; Hikihara and Kawagoshi, 1996; Moon and Holmes, 1979). Figure 1 provides a photograph and schematic of the experimental system examined in the research. A piezoelectric beam (PPA-2014; Midé Technology) is used as the energy harvester structure. The device is composed of layers of PZT-5H, copper, and glass-reinforced epoxy FR4; this composition results in appreciable inherent mechanical damping due to both the laminated design and the FR4 in particular. This beam is clamped at one end of a rigid aluminum mount. Attached to the free end of the cantilever are steel extensions, with total mass $m = 9$ g, that reduce the lowest order natural frequency of the beam and provide for a ferromagnetic material for the magnets to act upon. The total length of the cantilever and extension is $L = 61$ mm. A pair of neodymium magnets is positioned near the ferromagnetic extension, which cause attractive forces that work in opposite directions to linear elastic forces induced in the beam by displacement of the beam tip (Moon and Holmes, 1979). By reducing the distance between the beam tip and magnets, δ, and the distance between the magnets, Δ, the energy harvester may become bistable, thus maintaining one of two statically stable equilibria. In this work, the bistable nonlinearity is focused upon in the investigations, although the model framework composed for study is extensible to the significantly greater class of smooth, stiffness-based nonlinearities. As shown in Figure 1(b), the electrical leads from the energy harvester are connected to a standard diode bridge (1N4148 diodes). After the bridge, the DC flows through a parallel arrangement of filtering capacitor C_r and resistive load R, across which the rectified voltage, and DC power, are evaluated.

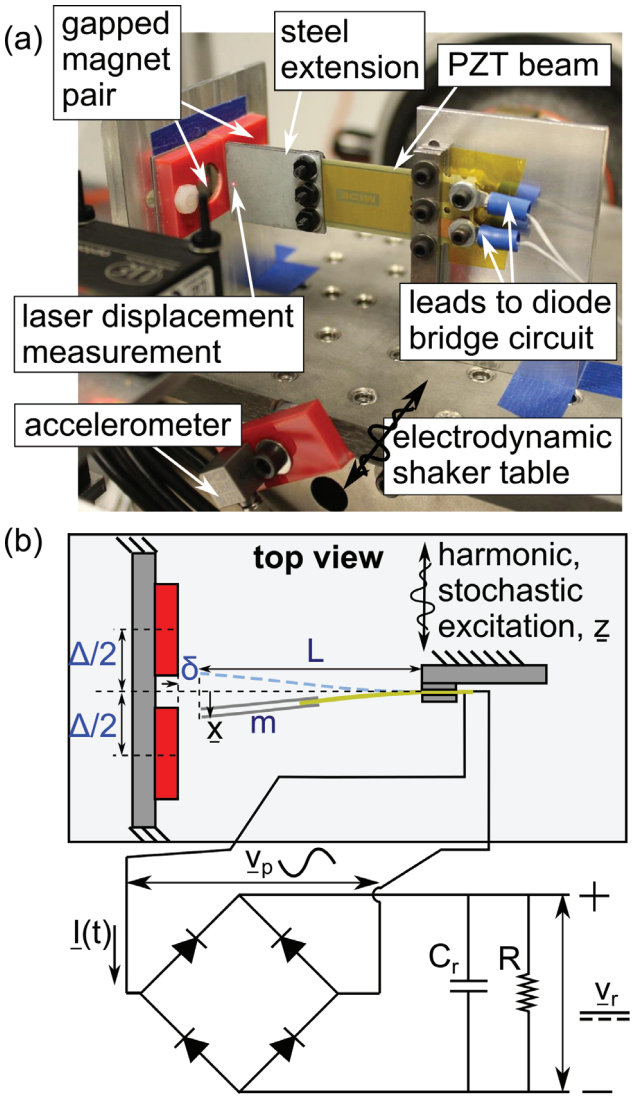

Figure 1. (a) Photograph and (b) schematic of experimental setup.

Governing equations

Considering that the nonlinear energy harvester exhibits a weak mono- or bistable nonlinearity, has a lowest order mode at a frequency much less than higher order modes, and is excited at frequencies near to this lowest order mode, the governing equations for this system are shown to be (Harne and Wang, 2014a; Moon and Holmes, 1979; Panyam et al., 2014)

$$m\ddot{\underline{x}} + c\dot{\underline{x}} + k_1(1-p)\underline{x} + k_3\underline{x}^3 + \alpha\underline{v}_p = -m\ddot{\underline{z}} \quad (1a)$$

$$C_p\dot{\underline{v}}_p + \underline{I} = \alpha\dot{\underline{x}} \quad (1b)$$

The assumptions described above are all borne out in the ensuing experimentation. In equation (1), $\underline{x}$ is the relative displacement of the energy harvester tip (i.e. the end of the extension in the experimental platform) with respect to the motion of the base $\underline{z}$ to which the clamped end of the harvester is attached; m, c, k_1, k_3 are the contributions from the cantilever mass, viscous damping, linear, and nonlinear stiffness to lowest order mode dynamics; p is referred to as a load parameter

since it characterizes the significance of magnetic force influence on reducing the linear stiffness similar to an axial compressive load (Moon and Holmes, 1979); C_p is the internal capacitance of the harvester; $\underline{v}_p$ is the voltage across the piezoelectric beam electrodes; α is the electromechanical coupling constant; and the overdot operator denotes differentiation with respect to time t.

The diode bridge AC–DC converter is connected to the energy harvester as shown in Figure 1(b). Here, perfect rectification is assumed. $\underline{I}(t)$ is the AC that flows into the diode bridge and is related to the rectified voltage $\underline{v}_r$ through (Shu and Lien, 2006a)

$$\underline{I}(t) = \begin{cases} C_r\dot{\underline{v}}_r + \dfrac{\underline{v}_r}{R};\ \text{if } \underline{v}_p = \underline{v}_r \\ -C_r\dot{\underline{v}}_r - \dfrac{\underline{v}_r}{R};\ \text{if } \underline{v}_p = -\underline{v}_r \\ 0;\ \text{if } \left|\underline{v}_p\right| < \underline{v}_r \end{cases} \tag{2}$$

To maintain a steady rectified voltage $\underline{v}_r$ for the load, which may be used for supplying a sensor or charging a temporary battery reserve, a sufficiently large capacitor C_r is needed (Shu and Lien, 2006a) so that the electrical time constant RC_r is much larger than the period of mechanical oscillation.

Non-dimensionalization of the governing equations assists in the acquisition of explicit analytical solutions via computationally efficient algorithms. Here, a new non-dimensionalization approach is introduced due to the presence of nonlinearities in the energy harvesting structure and in the rectifying circuit. After non-dimensionalization, the governing equations become

$$x'' + \eta x' + (1-p)x + \beta x^3 + \kappa v_p = -z'' \tag{3a}$$

$$v_p' + I = \theta x' \tag{3b}$$

$$I(\tau) = \begin{cases} \gamma v_r' + \rho v_r;\ \text{if } v_p = v_r \\ -\gamma v_r' - \rho v_r;\ \text{if } v_p = -v_r \\ 0;\ \text{if } \left|v_p\right| < v_r \end{cases} \tag{3c}$$

The corresponding non-dimensional parameters are defined as follows

$$\tau = \omega_0 t;\ \omega_0 = \sqrt{k_1/m};\ z = \underline{z}/x_0$$

$$\beta = k_3 x_0^2/k_1;\ \eta = c/m\omega_0;$$
$$\kappa = \alpha V_0/k_1 x_0;\ \gamma = C_r/C_p;$$
$$\rho = 1/C_p R\omega_0;\ \theta = \alpha x_0/C_p V_0$$

where x_0, V_0 are characteristic length and voltage, such that $x = \underline{x}/x_0$, $v_p = \underline{v}_p/V_0$, and $v_r = \underline{v}_r/V_0$. Here, $()'$ indicates differentiation with respect to non-dimensional time τ.

In order to analytically investigate realistic combinations of excitations on the nonlinear energy harvester for the first time, the base acceleration excitation includes harmonic and stochastic components

$$-z'' = a\cos\omega\tau + \sigma w(\tau) \tag{4}$$

such that $w(\tau)$ is a Gaussian white noise process with

$$\langle w(\tau)\rangle = 0 \ \text{ and } \ \langle w(\tau)w(\tau+\tau_0)\rangle = \delta(\tau_0) \tag{5}$$

and where σ is the normalized standard deviation of the noise (Roberts and Spanos, 1990). Considering the harmonic excitation component, a is the normalized base excitation magnitude and ω is the angular frequency of excitation $\underline{\omega}_0$ normalized with respect to ω_0. Thus, the absolute base excitation magnitude and standard deviation are $\underline{a} = ax_0k_1/m$ and $\underline{\sigma} = \sigma x_0 k_1/m$, respectively.

Approximate analytical solution to governing equations

By leveraging both harmonic and stochastic linearization, a strategy to predict mechanical responses of post-buckled structures was recently introduced (Harne and Dai, 2017). Yet, in the current context of vibration energy harvesting, the prior analysis is insufficient since it does not account for electrodynamic responses and has no means of characterizing DC power delivery. This research thus builds significantly beyond the prior work (Harne and Dai, 2017) for a comprehensive and first analysis suitable for nonlinear energy harvesters subjected to arbitrary harmonic and stochastic excitations.

To begin, a linearized governing equation system is created to approximate the influences of the nonlinearities in equation (3). Since the nonlinearity is present only in equation (3a), the equivalent linear system is governed by

$$x'' + \eta x' + \omega_e{}^2 x + \varepsilon + \kappa v_p = -z'' \tag{6a}$$

$$v_p' + I = \theta x' \tag{6b}$$

$$I(\tau) = \begin{cases} \gamma v_r' + \rho v_r;\ \text{if } v_p = v_r \\ -\gamma v_r' - \rho v_r;\ \text{if } v_p = -v_r \\ 0;\ \text{if } \left|v_p\right| < v_r \end{cases} \tag{6c}$$

The parameter ω_e^2 is an equivalent linear natural frequency while ε is an equivalent offset of displacement that exists if the nonlinearity induces bistability. Specifically, for bistable nonlinearities in the energy harvester, $\varepsilon = 0$ corresponds to snap-through responses that are symmetric about the unstable equilibrium, while $\varepsilon \neq 0$ correspond to intrawell responses that oscillate with low displacement amplitude around one of the non-zero stable equilibria. To determine the relations between these parameters and the original parameters of the exact governing equation system (equation (3)), the mean-square error E between equations (3a) and (6a) is minimized

$$E = (1-p)x + \beta x^3 - \omega_e^2 x - \varepsilon \tag{7}$$

The mean-square error occurs when $\partial\langle E^2\rangle/\partial\omega_e^2 = 0$ and $\partial\langle E^2\rangle/\partial\varepsilon = 0$ (Roberts and Spanos, 1990). By taking advantage of the linearized governing equations (equation (6)), to derive such relations, the mechanical and electronical responses are assumed to be composed from a pair of contributions strictly associated with either the harmonic or stochastic excitation components (equation (4)). A similar concept has been established to predict mechanical responses of post-buckled oscillators that are subjected to combined harmonic and stochastic excitation (Harne and Dai, 2017). Here, this concept is significantly extended to consider the overall electrodynamic responses of nonlinear energy harvesters, including DC power delivery, according to the requirements to account for the intricate electromechanical coupling and rectification stages. Using subscript h to denote the harmonic contribution and r to denote the random or stochastic contribution, one has

$$x(\tau) = x_h(\tau) + x_r(\tau) \tag{8a}$$

$$v_p(\tau) = v_{p,h}(\tau) + v_{p,r}(\tau) \tag{8b}$$

$$v_r(\tau) = v_{r,h}(\tau) + v_{r,r}(\tau) \tag{8c}$$

Note that the components associated with the white noise have zero-mean, $\langle x_r\rangle = \langle v_{p,r}\rangle = \langle v_{r,r}\rangle = 0$. The harmonic components are written by a Fourier series expansion associated with the normalized frequency of the base acceleration, while $v_{r,h}(\tau)$ is assumed to be constant

$$\begin{aligned} x_h(\tau) &= k(\tau) + h(\tau)\sin\omega\tau + g(\tau)\cos\omega\tau \\ &= k(\tau) + n(\tau)\cos[\omega\tau - \phi(\tau)] \end{aligned} \tag{9}$$

$$v_{p,h}(\tau) = p(\tau)\sin\omega\tau + q(\tau)\cos\omega\tau \tag{10}$$

The coefficients k, h, and g vary slowly in time, while $n^2 = h^2 + g^2$ and $\tan\phi = h/g$. If the energy harvester exhibits a bistable nonlinearity, the constant coefficient k is required to realize the displacement bias while the piezoelectric voltage associated with the harmonic base acceleration does not require such accounting according to equation (3b). Then, the mean-square error is minimized when

$$\frac{\partial\langle E^2\rangle}{\partial\omega_e^2} = \langle (1-p)x^2 - \omega_e^2 x^2 + \beta x^4 - \varepsilon x\rangle = 0 \tag{11a}$$

$$\frac{\partial\langle E^2\rangle}{\partial\varepsilon} = \langle (1-p)x - \omega_e^2 x + \beta x^3 - \varepsilon\rangle = 0 \tag{11b}$$

Substitution of the assumed solution equation (8a) into equation (11) enables the determination of ω_e^2 and ε (Ibrahim, 1985)

$$\omega_e^2 = (1-p) + \frac{3}{4}\beta\frac{n^4 + 8n^2\langle x_r^2\rangle + 8\langle x_r^2\rangle^2 + 4k^2\left(n^2 + 2\langle x_r^2\rangle\right)}{n^2 + 2\langle x_r^2\rangle} \tag{12}$$

$$\varepsilon = \frac{1}{4}\beta k\frac{3n^4 - 8k^2\left(n^2 + 2\langle x_r^2\rangle\right)}{n^2 + 2\langle x_r^2\rangle} \tag{13}$$

Because equation (6) is linear, the combined response of the linearized system is the superposition of responses individually associated with the harmonic or stochastic excitation components. Thus, the simultaneous solution to equations (14) and (15) enables the determination of the unknowns within the assumed solution forms of equation (8)

$$x_h'' + \eta x_h' + \omega_e^2 x_h + \varepsilon + \kappa v_{p,h} = a\cos\omega\tau \tag{14a}$$

$$v_{p,h}{}' + I_h = \theta x_h{}' \tag{14b}$$

$$I_h(\tau) = \begin{cases} \gamma v_{r,h}{}' + \rho v_{r,h};\ \text{if } v_{p,h} = v_{r,h} \\ -\gamma v_{r,h}{}' - \rho v_{r,h};\ \text{if } v_{p,h} = -v_{r,h} \\ 0;\ \text{if } |v_{p,h}| < v_{r,h} \end{cases} \tag{14c}$$

$$x_r'' + \eta x_r' + \omega_e^2 x_r + \varepsilon + \kappa v_{p,r} = \sigma w(\tau) \tag{15a}$$

$$v_{p,r}{}' + I_r = \theta x_r' \tag{15b}$$

$$I_r(\tau) = \begin{cases} \gamma v_{r,r}{}' + \rho v_{r,r};\ \text{if } v_{p,r} = v_{r,r} \\ -\gamma v_{r,r}{}' - \rho v_{r,r};\ \text{if } v_{p,r} = -v_{r,r} \\ 0;\ \text{if } |v_{p,r}| < v_{r,r} \end{cases} \tag{15c}$$

Harmonic electromechanical dynamics

To predict the harmonic electromechanical dynamics of the nonlinear energy harvester coupled to the rectifying circuit, we build upon a strategy devised by Liang and Liao (2012) that was developed for linear energy harvesting platforms. Introducing a total phase $\omega\Phi = \omega\tau - \phi$, the periodic voltage $v_{p,h}$ is presented in Figure 2 as the solid green curve. When the displacement x_h reaches a peak, the $v_{p,h}$ begins to fall from the level of the rectified voltage $v_{r,h}$ until the time at which the condition of equation (14c) is met for the negative value of the $v_{p,h}$ that matches the absolute value of the steady-state rectified voltage.

Considering the sinusoidal form of the electromechanical responses and the switching conditions of equation (14c), the harmonic voltage across the piezoelectric electrodes $v_{p,h}$ is expressed

$$v_{p,h}(\omega\Phi) = \begin{cases} \theta n[\cos\omega\Phi - 1] + v_{r,h};\ 0 < \omega\Phi \le \Theta \\ -v_{r,h};\ \Theta < \omega\Phi \le \pi \\ \theta n[\cos\omega\Phi + 1] - v_{r,h};\ \pi < \omega\Phi \le \pi + \Theta \\ v_{r,h};\ \pi + \Theta < \omega\Phi \le 2\pi \end{cases} \tag{16}$$

As shown in Figure 2, Θ corresponds to the phase angle at which current flow changes from the blocked

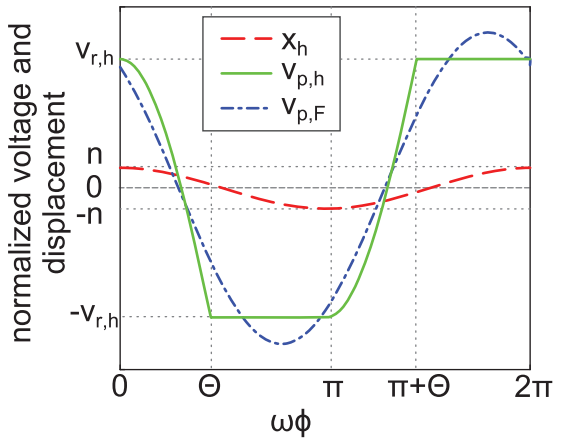

Figure 2. Representation of single period of voltage across the piezoelectric and displacement of the energy harvester, as adapted from Liang and Liao (2012).

to passing states. Using equation (16), this phase is found to be

$$\cos\Theta = 1 - \frac{2v_{r,h}}{\theta n} \tag{17}$$

according to the continuity of the piecewise functions. To leverage the harmonic steady-state assumptions of equation (14), a sinusoidal form of equation (16) is required. Thus, $v_{p,h}$ is approximated by its fundamental terms of its Fourier series expansion. Using the fact that for one-half cycle of the steady-state behaviors (Figure 2) the electromechanical responses oscillate from peak-to-peak (Shu and Lien, 2006a), one finds

$$\int_0^{\pi} v_{p,h}{}' - \theta x' d(\omega\Phi) = -2v_{r,h}\omega + 2\theta n\omega \tag{18}$$

In addition, assuming that the rectified voltage change per cycle is negligible compared to the mean value, an energy balance yields

$$\int_0^{\pi} \gamma v_{r,h}{}' + \rho v_{r,h} d(\omega\Phi) = \pi\rho v_{r,h} \tag{19}$$

Therefore, integrating equation (14c) in a semi-period yields

$$v_{r,h} = \frac{2\theta}{\frac{\pi}{\omega}\rho + 2} n \tag{20}$$

Consequently, the DC power associated with the harmonic base acceleration is

$$P_h = \frac{v_{r,h}{}^2}{R} = \frac{4\theta^2}{R\left(\frac{\pi}{\omega}\rho + 2\right)^2} n^2 \tag{21}$$

Then, the first-order time-harmonic of $v_{p,F}$ is found by the fundamental term of the Fourier series of equation (16) using equation (20)

$$v_{p,F}(\tau) = \left[\frac{-g(\tau)}{\pi}\theta\sin^2\Theta + \frac{h(\tau)\theta}{2\pi}(2\Theta - \sin 2\Theta)\right]\sin\omega\tau + \left[\frac{h(\tau)}{\pi}\theta\sin^2\Theta + \frac{g(\tau)\theta}{2\pi}(2\Theta - \sin 2\Theta)\right]\cos\omega\tau \tag{22}$$

The prior steps to yield equation (22) are comparable to the prior work (Liang and Liao, 2012). Yet, to leverage equation (22) for the nonlinear energy harvesting system of interest here, continued steps are required to provide meaningful predictions of the dynamic response. By virtue of the assumption of single harmonic response, it is here assumed that $v_{p,F}(\tau) \approx v_{p,h}(\tau)$. Then, using all of the assumed, harmonic electromechanical responses, the coefficients of the constant, $\sin\omega\tau$, $\cos\omega\tau$ terms are collected from substitution of the response forms into equation (14a)

$$-\eta k' = \omega_e{}^2 k + \varepsilon \tag{23a}$$

$$-\eta h' + 2\omega g' = \Lambda h - \mathrm{X} g \tag{23b}$$

$$-2\omega h' - \eta g' = \Lambda g + \mathrm{X} h - a \tag{23c}$$

where

$$\Lambda = \left(\omega_e{}^2 - \omega^2\right) + \frac{\theta\kappa}{2\pi}(2\Theta - \sin 2\Theta);\ \mathrm{X} = \eta\omega + \frac{\theta\kappa}{\pi}\sin^2\Theta \tag{24}$$

Under steady-state conditions such that the time variations on the left-hand side of equation (23) vanish, one determines that

$$k^2 = 0 \text{ or } k^2 = \frac{\varepsilon^2}{\omega_e^4} = -\frac{3}{2}n^2 - 3\langle x_r^2\rangle - (1-p)/\beta \tag{25}$$

Then, equations (23b) and (23c) together yield

$$[\Lambda^2 + \mathrm{X}^2]n^2 = a^2 \tag{26}$$

Equation (26) is a cubic polynomial in terms of n^2. The complex roots and negative real roots of equation (26) are therefore not physically meaningful.

Stochastic electromechanical dynamics

Equation (26) characterizes the harmonic displacement response of the nonlinear energy harvester, out of which the corresponding piezoelectric beam voltage and rectified voltage are, respectively, computed from equations (22) and (20). Yet, it is seen that the polynomial of equation (26) is a function of the equivalent linear natural frequency ω_e which itself is a function of the mean-square displacement $\langle x_r\rangle$ associated with the stochastic

excitation component. Therefore, by the linearization approach to equation (6), the harmonic and stochastic contributions become intertwined in the analysis. As a result, with solutions to the harmonic-related equation system (equation (14)), the stochastic-related equation system (equation (15)) is addressed.

To determine relations among the mean-square nonlinear harvester displacement $\langle x_r \rangle$ and the piezoelectric $v_{p,r}$ and rectified $v_{r,r}$ voltages, a new empirical approach is undertaken. Specifically, a large number of simulations are evaluated using a range of non-dimensional parameters ρ and γ where a non-dimensional beam velocity x_r' is prescribed using zero-mean white noise. Considering the assumption of linearity, one has that $\left\langle (x_r^2)' \right\rangle \approx \langle x_r^2 \rangle \omega_e^2$. Fitting the results with surfaces among ρ, γ, and $\langle x_r \rangle$, the following relationships are revealed

$$\langle v_{p,r}{}^2 \rangle \approx \frac{200 \langle x_r^2 \rangle {\omega_e}^2}{3\rho^2 + 6\rho + \frac{\gamma^{1.5}}{2000}} \tag{27}$$

$$\langle v_{r,r}{}^2 \rangle \approx \sqrt{2} \langle v_{p,r}{}^2 \rangle \tag{28}$$

With equations (27) and (28), of the system equation (15) only equation (15a) requires solution. Yet, this equation is not amenable to straightforward solution. A second linear approximation is then made, assuming a new equivalent natural frequency ω_{en}, which assists to approximate equation (15a) by

$$x_r'' + \eta x_r' + {\omega_{en}}^2 x_r = \sigma w(\tau) \tag{29}$$

The error between equations (15a) and (29) is

$$E_n = {\omega_e}^2 x_r + \kappa v_{p,r} - {\omega_{en}}^2 x_r \tag{30}$$

Using the same procedures as in the prior section, one has

$$\frac{\partial \langle {E_n}^2 \rangle}{\partial \omega_{en}^2} = \frac{\partial \left\langle {\omega_e}^4 {x_r}^2 - 2{\omega_e}^2 {\omega_{en}}^2 {x_r}^2 + {\omega_{en}}^4 {x_r}^2 + 2\kappa({\omega_e}^2 - {\omega_{en}}^2) v_{p,r} x_r + {v_{p,r}}^2 \kappa^2 \right\rangle}{\partial \omega_{en}^2} = 0 \tag{31}$$

Toward solving equation (31), the expectation of the product of x_r and $v_{p,r}$ is taken according to the covariance process (Soong, 2004)

$$E\left[x_r v_{p,r}\right] = \mathrm{std}(x_r)\mathrm{std}\left(v_{p,r}\right) = \sqrt{\frac{200}{3\rho^2 + 6\rho + \frac{\gamma^{1.5}}{2000}}} \langle x_r^2 \rangle \omega_e \tag{32}$$

Consequently, the new equivalent natural frequency is

$${\omega_{en}}^2 = {\omega_e}^2 + \kappa \omega_e \sqrt{\frac{200}{3\rho^2 + 6\rho + \frac{\gamma^{1.5}}{2000}}} \tag{33}$$

Thereafter, the mean-square displacement $\langle x_r \rangle$ induced by the zero-mean, white noise base excitation component is (Bulsara et al., 1982)

$$\langle x_r^2 \rangle = \frac{\sigma^2}{2\eta\omega_{en}^2} \tag{34}$$

With equation (34), the piezoelectric and rectified voltages associated with the stochastic excitation are found from equations (27) and (28), respectively.

Combined harmonic and stochastic response of the nonlinear energy harvester

Considering the prior analytical formulation and nonlinear coupling of equations, equations (12), (26), and (34) must be simultaneously solved to compute the total response of the energy harvester when subjected to a combination of harmonic and stochastic base acceleration. Then, by equation (8), the total responses may be reconstructed.

In addition to the response forms reconstructed in equation (8), specific measures are useful to characterize the energy harvesting performance of the nonlinear platform. For instance, one meaningful measure is the total mean-square displacement

$$\langle x^2 \rangle = \langle x_h^2 \rangle + \langle x_r^2 \rangle = k^2 + \frac{1}{2}n^2 + \langle x_r^2 \rangle \tag{35}$$

The total mean-square voltage across the piezoelectric electrodes is given by equation (36). Finally, the total mean-square rectified voltage across the resistive load R is computed from equation (37) which leads to the determination of the total DC power delivery to the load via equation (38)

$$\langle {v_p}^2 \rangle = \frac{1}{2}\left|v_{p,h}\right|^2 + \langle v_{p,r}{}^2 \rangle \tag{36}$$

$$\langle {v_r}^2 \rangle = {v_{r,h}}^2 + \langle v_{r,r}{}^2 \rangle \tag{37}$$

$$P = P_h + \frac{\langle {v_{r,r}}^2 \rangle}{R} \tag{38}$$

All together, the new analytical approach builds greatly from prior work that studies the harmonically excited response of linear energy harvesters coupled with rectifying circuits (Liang and Liao, 2012) and from prior work that studies the structural dynamics of post-buckled oscillators subjected to harmonic and stochastic excitations (Harne and Dai, 2017). Indeed, the analysis of this report enables the first approach to

explicitly predict the structural and electrical dynamics of nonlinear vibration energy harvesters subjected to arbitrary combinations of harmonic and stochastic excitations when coupled to rectifying circuit for DC power delivery.

Experimental methods

The experimental platform is shown in Figure 1(a). Laser displacement sensors (Micro Epsilon ILD-1420) measure the absolute cantilever tip displacement and absolute displacement of the electrodynamic shaker table. An accelerometer (PCB Piezotronics 333B40) also measures the shaker table acceleration in the same axis of motion. The base excitations are applied by a controlled electrodynamic shaker (LabWorks ET-140), as driven by an amplifier (LabWorks PA-141). The noise excitation component is defined as the variance of a normally distributed voltage time series that superimposes with a harmonic voltage time series, which together drive the shaker. The AC piezoelectric voltage across the electrodes of the energy harvester is recorded in addition to the rectified voltage evaluated over the resistive load. All channels of data are recorded at a sampling frequency of 4096 Hz and are thereafter digitally filtered from 1 to 500 Hz. The experimentally identified parameters of the nonlinear energy harvester and diode bridge circuit are provided in Table 1. As seen in the table, the load parameter p is greater than unity, which indicates that the energy harvester was subjected to enough magnetic force to induce bistability.

Table 1. Experimentally identified system parameters.

m (g)	b (N s/m)	k_1 (N/m)	p (dim)
9.45	0.125	160	1.75
k_3 (MN/m^3)	C_p (nF)	C_r (μF)	α (mN/V)
33	96	10	1.4

Results and discussions

In order to verify the analytical predictions, direct numerical simulations of the governing equations are carried out using fourth-order Runge–Kutta numerical integration with increased tolerances on adaptive time-stepping routines in the MATLAB software. Initial conditions for the states of the electromechanical system are chosen from normally distributed random numbers approximately within an order of magnitude of the ultimate response state amplitude. The analytical and numerical efforts are undertaken in parallel with experimentation, using the parameters identified from the experimental platform, as given in Table 1. To determine the natural frequencies associated with each low amplitude intrawell response and the damping constant, impulsive ring down responses are undertaken. It is ensured that the influences of the magnets upon the ferromagnetic beam tip are positioned such that the natural frequencies around both stable equilibria are identical to $\underline{\omega}_0$, thus leading to only parameters k_1 and k_3. The distance between statically stable equilibria is measured, $2x^*$. Using classical relations, the equivalent mass of the harvester m is determined by considering it to be a cantilever with tip mass, while the linear stiffness k_1 is similarly identified according to the piezoelectric beam properties and dimensions. With this information, the load parameter is computed as $p = 1 + \underline{\omega}_0^2 m/2k_1$ for $x^* \neq 0$ and as $p = 1 - \underline{\omega}_0^2 m/k_1$ for $x^* = 0$. Finally, the nonlinear stiffness k_3 is determined from $k_3 = k_1(p-1)/(x^*)^2$ for $x^* \neq 0$ which is the relevant case of this research that gives attention to the bistable nonlinearity of the energy harvester. For monostable energy harvesters, the determination of the nonlinear stiffness k_3 can be achieved using data from forced excitation experiments (Rao, 2004).

The following paragraphs present the collective analytical, numerical, and experimental results that enable the detailed study of excitation and electrical parameter influences upon the nonlinear energy harvester DC power delivery.

Electromechanical responses induced by pure harmonic excitation

As a limiting case of the model predictions, the vibration energy harvester is first subjected to base acceleration of amplitude $\underline{a} = 7.5\,\mathrm{m/s^2}$ without noise contribution $\underline{\sigma} = 0$. The linearized natural frequency of the bistable nonlinear energy harvester is around 25.36 Hz, and the frequencies of the harmonic excitation are applied around this resonant state.

For this excitation condition, Figure 3(a) and (b) presents the analytical (curves) and numerical (data points) results of the beam tip harmonic displacement amplitude and average charging power, respectively, while the corresponding experimental measurements are shown in Figure 3(c) and (d). According to the analytical and simulation results, for harmonic excitation frequencies less than around 20 Hz, the bistable energy harvester may exhibit either the large amplitude snap-through dynamics or the low amplitude "intrawell" responses associated with oscillations around one or the other stable equilibria. Such coexistence of dynamic regimes is revealed by more than one analytical prediction or numerical simulation data point for the same harmonic excitation frequency less than about 20 Hz, in Figure 3(a) and (b). At higher frequencies, only the low amplitude oscillation is found. Together, the analytical and numerical results are in overall good agreement across the whole frequency range, excepting

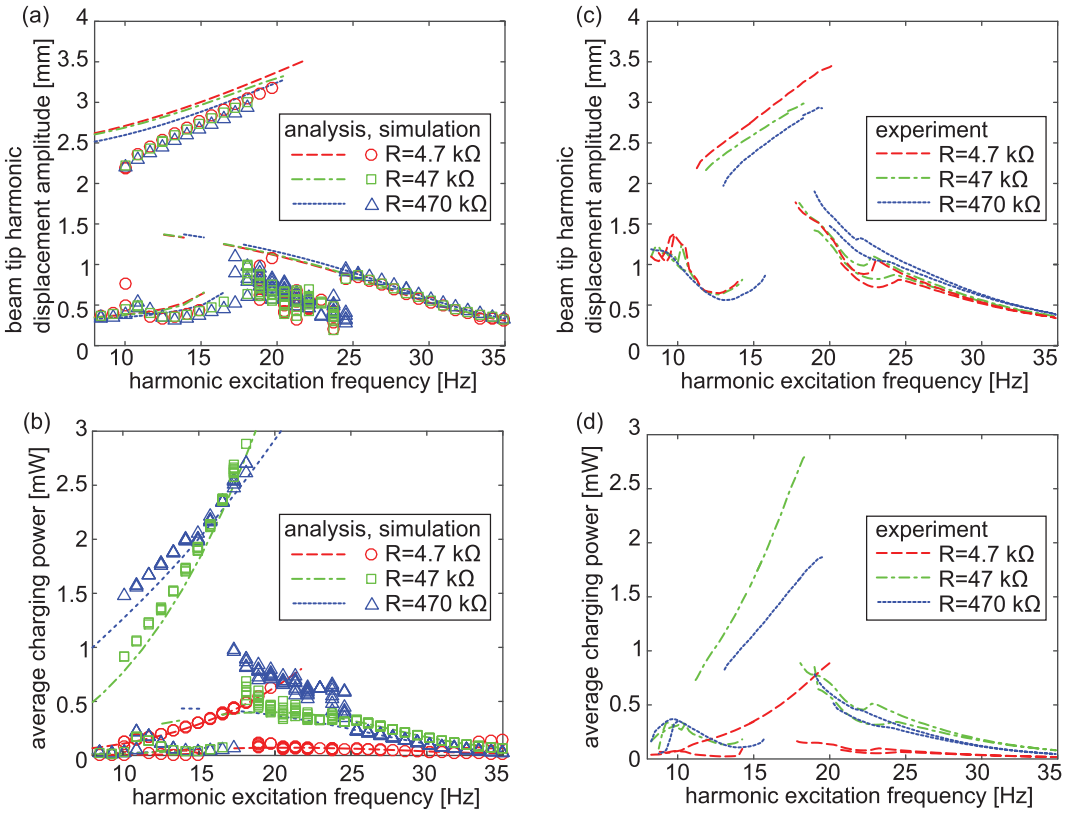

Figure 3. Analytical prediction (in lines) and simulated results (in shapes) of (a) beam tip harmonic displacement magnitude at the harmonic excitation frequency and (b) average charging power across resistive loads R, under pure harmonic excitation with amplitude $\underline{a} = 7.5\,\mathrm{m/s^2}$. Corresponding experimental measurements are shown in (c, d).

around 20–25 Hz where the simulations suggest aperiodic or chaotic states of vibration may occur, which the analysis is unable to predict by virtue of steady-state assumptions. Considering these different dynamic regimes, it is clear from Figure 3(b) that the snap-through dynamics are the favored behavior for enhancing DC power delivery. Indeed, in Figure 3, a range of load resistances is considered: $R = [4.7,\ 47,\ 470]\,\mathrm{k\Omega}$. By change of the resistance from 4.7 to 47 kΩ and then to 470 kΩ, the activation of the snap-through response is suppressed across portions of the harmonic excitation frequency bandwidth. More importantly, considering this large range of resistance, an optimal value is suggested. Namely, the peak DC power generation increases from around 0.62 mW using a resistance of 4.7 kΩ to around 2.88 mW using 47 kΩ; then by increasing the resistance still further to 470 kΩ, the peak power reduces to just 2.70 mW. These trends are in good agreement between the simulations and theoretical predictions, providing strong verification to the analytical formulation created here.

In the corresponding series of experiments, harmonic base acceleration is applied with slowly sweeping frequency from low to high and then high to low values at a rate of 0.09 Hz/s. The experimental results shown in Figure 3(c) and (d) are in good qualitative and quantitative agreement with the model findings. In particular, the potential for an optimal resistance for DC power delivery is also apparent in the measurements since the resistor of 47 kΩ provides the highest peak DC power among the three values of resistances examined. Also, the bandwidth of the snap-through dynamic regime is suppressed by increase in the resistance, which is likewise revealed both analytically and numerically.

Overall, the results of Figure 3 establish that the analytical model accurately reproduces the electrodynamic behaviors of the bistable nonlinear energy harvester under the limiting case of pure harmonic excitation. The following section examines the influence of the additive stochastic excitation contribution on the dynamic response and DC power generation.

Nonlinear energy harvesting under combined harmonic and stochastic excitations: case example

Then, in addition to the harmonic amplitude of base acceleration $\underline{a} = 7.5\,\mathrm{m/s^2}$, stochastic noise is introduced with standard deviation $\underline{\sigma} = 11.25\,\mathrm{m/s^2}$ to result in the overall combined excitation form that acts on the nonlinear harvester. In other words, the ratio of noise standard deviation to harmonic amplitude is approximately

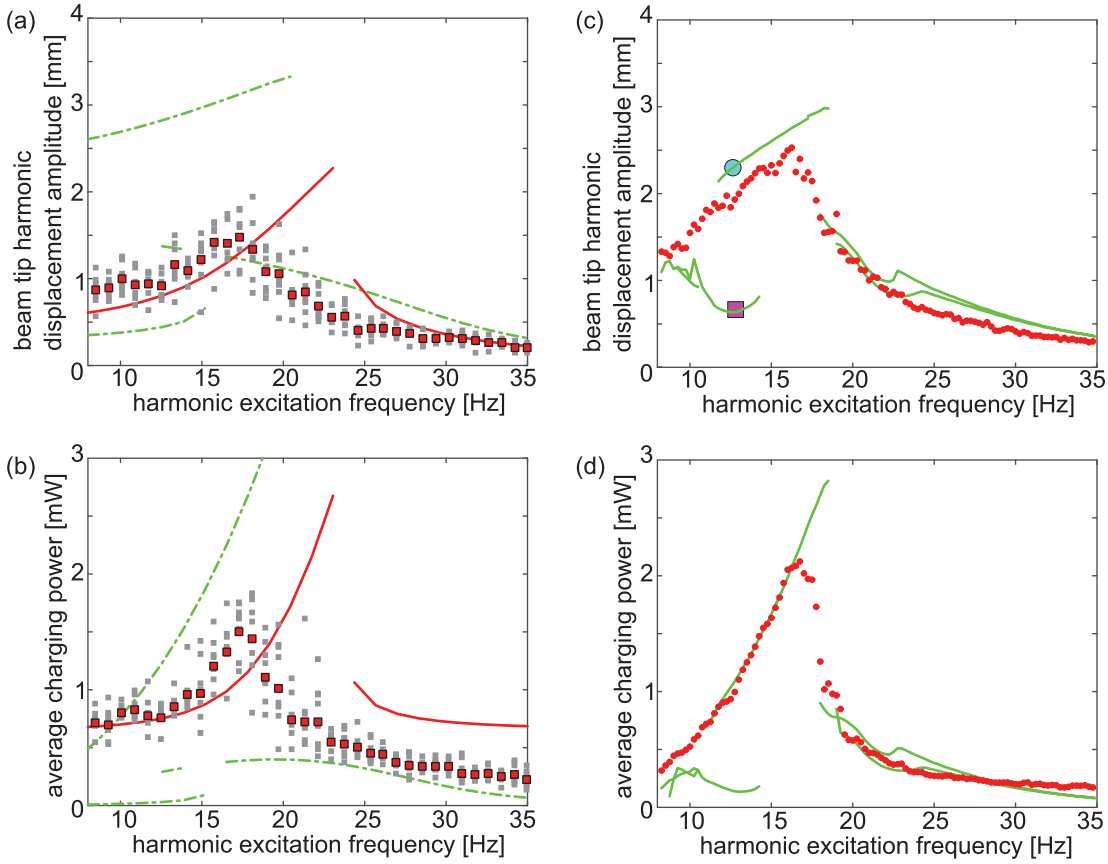

Figure 4. Analytical predictions and numerical simulations of (a) beam tip harmonic displacement magnitude at the harmonic excitation frequency, (b) average charging power across resistive loads $R = 47\ \text{k}\Omega$, with harmonic excitation amplitude $\underline{a} = 7.5\ \text{m/s}^2$. Dash-dot curves indicate responses without stochastic excitation, $\underline{\sigma} = 0$. Thick solid curves indicate response with noise $\underline{\sigma} = 11.25\ \text{m/s}^2$. Small squares and filled large squares are, respectively, the individual and means results of numerical simulations conducted at each excitation frequency. Corresponding experimental measurements are shown in (c, d). Solid curves indicate responses without stochastic excitation, $\underline{\sigma} = 0$, while filled circles indicate response with noise $\underline{\sigma} = 11.25\ \text{m/s}^2$.

3/2. To provide an easier visualization of the different cases of excitation, the following results only consider the case when the load resistance is $R = 47\ \text{k}\Omega$ while the excitations are either purely harmonic or include the noise to harmonic excitation ratio of 3/2.

In Figure 4(a) and (b), the analytical results are shown for the pure harmonic case (dashed-dot curves) and for the case with the additive noise (solid curves). Figure 4(a) and (b) shows the beam tip harmonic displacement amplitude and the average charging power, respectively. As shown in Figure 4(a) and (b), the numerical results are shown as gray data points for all of the simulations and as filled red squares for the averages of the simulations at any specific harmonic excitation frequency. Figure 4(c) and (d) presents the corresponding experimental findings, with the pure harmonic data sets indicated with solid curves and the short-time averages of the measurements under the combined harmonic and stochastic base excitations plotted as red filled circles.

According to the analytical predictions shown in Figure 4, due to the additive noise excitation component, the nonlinear harvester loses the ability to undergo coexistent responses, since only one dynamic regime is predicted analytically at any given frequency, across the bandwidth considered. This result is in agreement with the outcomes of the numerical simulations. The introduction of the stochastic excitation component causes the displacement amplitudes in Figure 4(a) to reduce considerably from the levels associated with harmonic snap-through, although the displacements are still greater than the low amplitude dynamic regime. The average charging powers shown in Figure 4(b) are correspondingly reduced; at frequencies less than about 20 Hz, the powers are approximately one-half of the levels achieved for the harvester when snap-through dynamics are triggered under pure harmonic excitation. Yet, the experimental measurements in Figure 4(c) do not discover as great of reduction in the response as predicted analytically and observed numerically. In particular, while the noise also suppresses the coexistence of the dynamic regimes, it does not as greatly impact the response amplitudes, whether considering the displacement or charging

power. One explanation for this difference between experiment and model is that the overall dissipation of energy in the harvester is modeled by a viscous damping. Yet, the piezoelectric beam used experimentally contains a significant proportion of glass-reinforced epoxy laminate, which is a viscoelastic material and as such leads to frequency- and rate-dependent damping properties (Fosdick et al., 1998; Ketema, 1998). Thus, the omission of viscoelastic damping in the current model may explain the difference between experimental measurements and model predictions, which encourages a more accurate model formulation in future to apply such a nonlinear energy harvester in practice. Despite such minor differences in the amplitudes of the displacement and DC comparing the model predictions and measurements, the experimental results are still in overall good agreement with analytical prediction as well as the numerical simulation. Thus, the theoretical formulation and solution procedure established here are sufficiently validated.

Considering the influence of the stochastic contribution to the overall base excitation upon the harvester, Figure 4(b) and (d), while the peak DC power delivery may be reduced, a favorable outcome is the elimination of the coexistence of low amplitude and snap-through dynamics at low frequencies. This results in a form of insurance to obtain a meaningful DC power level closer in value to the result achieved under pure harmonic excitation. Both model results and experimental measurements reveal such behaviors.

To look deeply at the impact of additive stochastic excitation, experimental time series at 13 Hz are presented in Figure 5. The time series of base acceleration is shown in Figure 5(a) with and without the stochastic component, recalling that the ratio of noise standard deviation to harmonic amplitude is 3/2, which explains the considerable differences between the two time series of base acceleration. The beam tip displacement time series is shown in Figure 5(b) and (d) while the corresponding voltages across the piezoelectric beam electrodes and across the load resistor $R = 47\ \text{k}\Omega$ are shown in Figure 5(c) and (e). For the low amplitude intrawell oscillation, Figure 5(b) and (c), the additive stochastic excitation provides a beneficial perturbation away from the low amplitude dynamic state, inducing greater mechanical response and hence rectified voltage. This is seen in Figure 5(b) and (c) comparing the time series response without noise (dashed or dotted curves) to those measures with noise (solid or dash-dot curves). The corresponding impact on the electromechanical snap-through dynamics are shown in Figure 5(d) and (e). According to Figure 5(d) and (e), the additional stochastic excitation slightly reduces peak-to-peak piezoelectric voltage generation, although the displacement amplitude is not reduced overall. Yet, because the snap-through response is perturbed from a steady state, the measurements show that the loss of rectified voltage results in an overall reduction in the charged voltage across the resistor, and hence less DC power.

DC power delivery for varied levels of stochastic excitation

As found from the results of the previous section, the additive stochastic excitation component may significantly change the electromechanical responses of the bistable nonlinear energy harvester. And as exemplified in the time series of Figure 5, the effects of the noise on the overall behavior are unique whether the underlying steady-state response is a coexistent low amplitude intrawell oscillation or the high amplitude snap-through dynamic. To closely investigate these influences, this section examines a wide range of stochastic excitation levels with respect to a fixed harmonic level of base excitation.

Figure 6 presents analytical, numerical, and experimental results obtained when the 13 Hz harmonic excitation amplitude is $\underline{a} = 2.85\,\text{m/s}^2$ while the ratio of the noise standard deviation to harmonic amplitude, $\underline{\sigma}/\underline{a}$, varies from 0 to 4.5. The value for the load resistor for these results is $R = 470\ \text{k}\Omega$. The analytical predictions are shown by blue solid (red dashed) curves in Figure 6(a) and (b) according to the snap-through (intrawell) responses for the harmonic displacement amplitude and charging power, respectively. Numerical and experimental results are, respectively, denoted by open and filled data points. All of the results agree that for low levels of noise, using this harmonic excitation amplitude, the nonlinear harvester exhibits the low amplitude intrawell response as the underlying steady state. Similar to the case of the role of the harmonic excitation frequency upon the harvester electromechanical dynamics, the analysis used to generate the results of Figure 6 also suggests that coexisting dynamic behaviors may exist for a given value of σ/a. Indeed, the analysis predicts that another low amplitude dynamic may occur for low levels of additive noise such as $\sigma/a < 1$, although neither simulations nor experiments detect its existence. This suggests that such additional dynamic behavior may have low likelihood of being induced in practice according to its basin of attraction (Harne and Wang, 2017). Nevertheless, the intrawell responses provide negligible DC power, as shown in Figure 6(b) for low noise levels.

As the noise standard deviation is increased respecting the harmonic amplitude of the excitation, the DC power gradually increases, with a significant growth observed analytically, numerically, and experimentally around a ratio of $\underline{\sigma}/\underline{a} = 2$. An explanation for this behavior is given by simulated and measured results in Figure 6(c) which plot the percentage of time that the beam undergoes the coexistent snap-through dynamic. Around $\underline{\sigma}/\underline{a} = 2$, this percentage clearly begins to

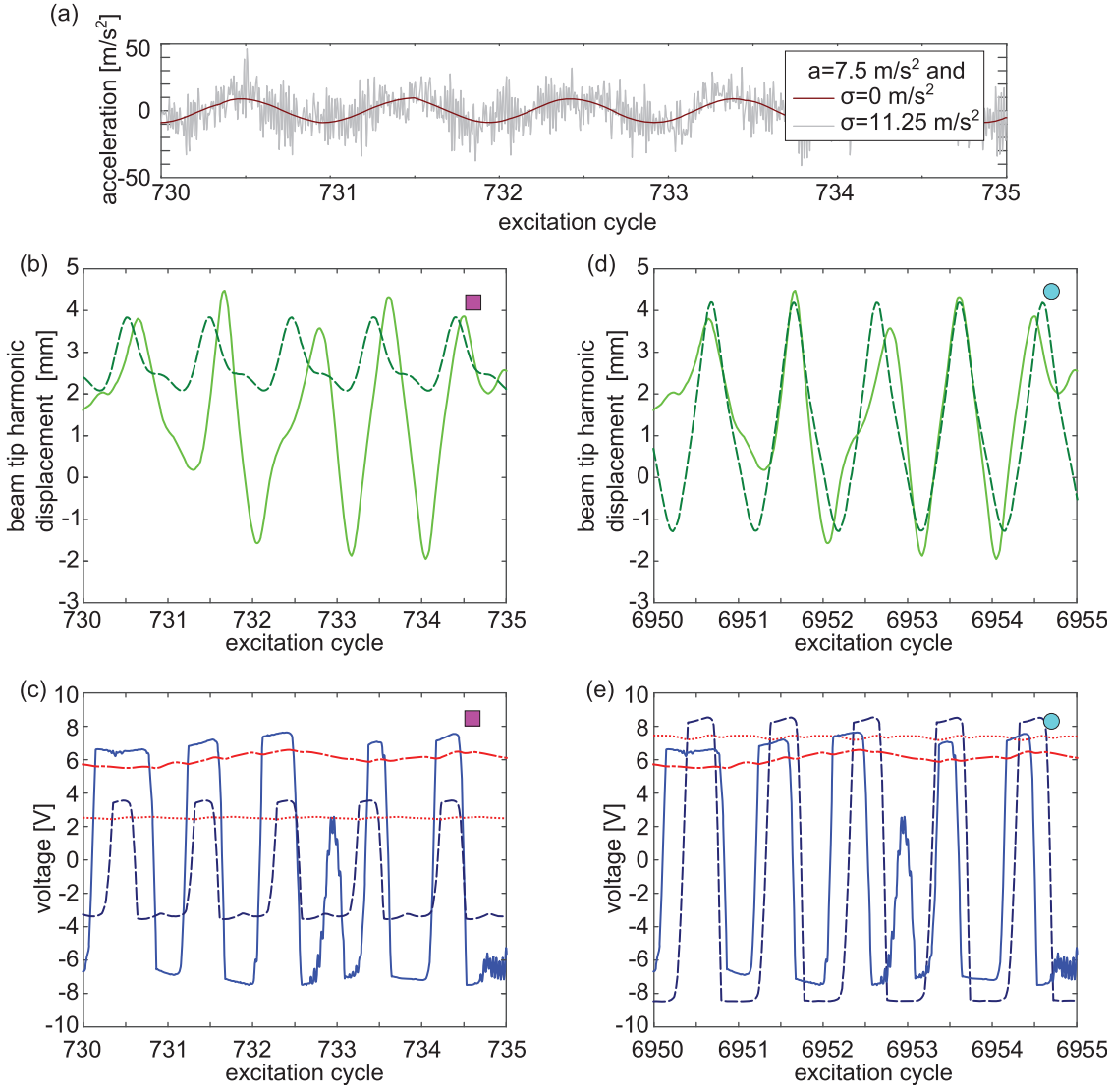

Figure 5. Portions of time series of experimental measurements for the (a) base accelerations provided to the energy harvester for harmonic-only and combined harmonic with stochastic excitations, (b, d) beam tip displacement without noise (dashed curves) and with noise $\underline{\sigma} = 11.25\,\mathrm{m/s^2}$ (solid curves), and (c, e) voltage from piezoelectric beam and rectified voltage across resistive load $R = 47\,\mathrm{k\Omega}$, without noise (dashed curves and dotted curves) and with noise $\underline{\sigma} = 11.25\,\mathrm{m/s^2}$ (solid curves and dash-dot curves). Results shown in (b, c) without noise correspond to the intrawell steady state indicated by the square data point in Figure 4(c), while results shown in (d, e) without noise correspond to the snap-through steady state indicated by the circle data point in Figure 4(c).

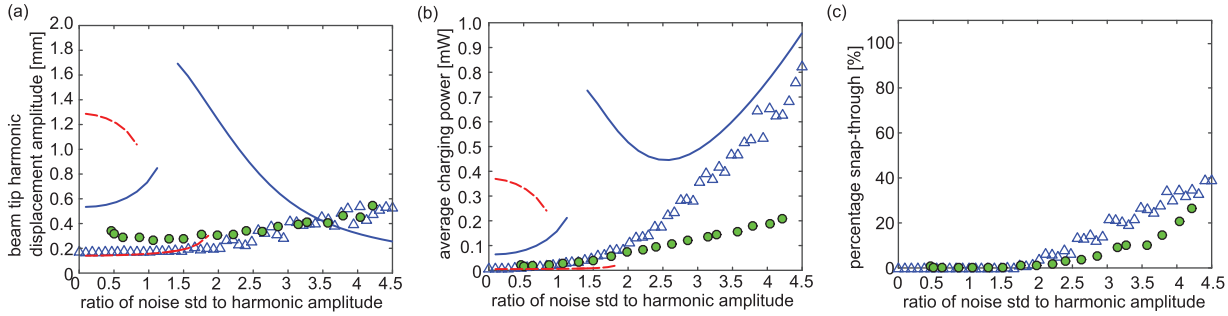

Figure 6. (a) Harvester harmonic displacement amplitude, (b) average charging power across resistive load $R = 470\,\mathrm{k\Omega}$, and (c) percentage of time that the beam spends snapping through, as a function of the ratio between noise standard deviation and harmonic amplitude of the base excitation. Blue solid (red dash) curves indicate analyzed responses associating with snap-through (intrawell) dynamics, blue triangles are the simulated results, and green filled circles indicate experimental measurements. In all cases, the harmonic excitation amplitude is $\underline{a} = 2.85\,\mathrm{m/s^2}$ while the frequency is 13 Hz.

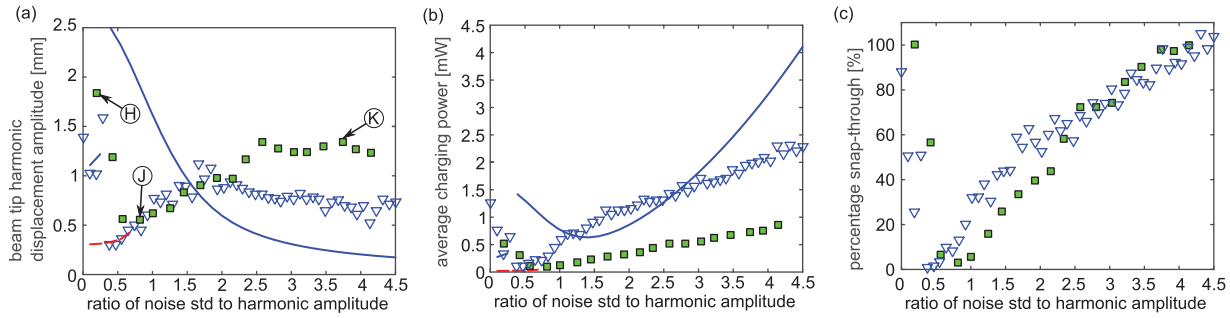

Figure 7. (a) Harvester harmonic displacement amplitude, (b) average charging power across resistive load R = 470 kΩ, and (c) percentage of time that the beam spends snapping through, as a function of the ratio between noise standard deviation and harmonic amplitude of the base excitation. Blue solid (red dash) curves indicate analyzed responses associating with snap-through (intrawell) dynamics, blue triangles are the simulated results, and green filled circles indicate experimental measurements. In all cases, the harmonic excitation amplitude is $\underline{a} = 5.85\,\mathrm{m/s^2}$ while the frequency is 13 Hz.

increase from near-zero values obtained for smaller ratios of excitation properties. This indicates that the noise begins to contribute favorably to DC power delivery provided by the harvester because the snap-through response is induced, even though the underlying steady-state response is a low amplitude intrawell behavior. The results of Figure 6 suggest that for harmonic amplitudes of base excitation that are insufficient to activate snap-through dynamics in the bistable nonlinear energy harvester, the DC power delivery may be considerably enhanced by the introduced of enough noise, here around $\underline{\sigma}/\underline{a}>2$, that triggers the desirable dynamic in a stochastic way, similar to the time series, as shown in Figure 5(c).

Figure 7 presents results considering greater amplitude of the harmonic base excitation, $\underline{a} = 5.85\,\mathrm{m/s^2}$, while all other notations and system parameters remain the same as the case shown in Figure 6. For this harmonic amplitude of base acceleration, in the absence of noise, the harvester exhibits the persistent snap-through response as the underlying steady-state behavior, similar to the time series show in Figure 5(d) and (e) derived from the measurements used to present Figure 4(c) and (d). It is plainly revealed in Figure 7(a) that the snap-through dynamic is inhibited by low levels of noise, specifically when the ratio of the noise standard deviation to amplitude of harmonic components is about $0<\underline{\sigma}/\underline{a}\leq 0.8$. Figure 7(b) shows that the DC power reduces greatly under such circumstances, when compared to the harmonic-only DC power output shown under the condition $\underline{\sigma}/\underline{a} = 0$.

These features are illuminated further by observing the time series of electromechanical response labeled as H and J in Figure 7(a). In Figure 8, the response labeled as H is shown in (a) for displacement and (b) for piezoelectric and charging voltages, which consider a case when the noise is insignificant in standard deviation when compared to the amplitude of the harmonic excitation. When the ratio $\underline{\sigma}/\underline{a}$ is increased closer to around 0.75, Figure 8(c) and (d) shows the corresponding displacement and voltage time series. Comparing these two cases of noise contribution to the overall base excitation, it is evident that the snap-through dynamic is suppressed for the case of $\underline{\sigma}/\underline{a}\approx 0.75$, leading to reduced charging voltage and hence less DC power delivery due to the reduced periodicity of the mechanical oscillations.

Studying the results of Figure 7(a) further, when the ratio $\underline{\sigma}/\underline{a}$ increases beyond around 0.75, the snap-through behavior is predicted by analysis to be the only dynamic regime triggered. Comparatively, as shown in Figure 7(c), the percentage of time that simulations and experiments observe the snap-through response increases significantly for ratios $\underline{\sigma}/\underline{a}$ greater than about 0.75, which supports the more idealized prediction by the analysis. Thus, large DC power delivery is recovered for greater noise contribution in the excitation. Figure 8(e) and (f) plots time series of displacement and voltage for the data point labeled as K in Figure 7(a). Interestingly, the displacement is clearly not a steady snap-through, although as shown in Figure 8(f) the rectified voltage is greater than the voltage achieved when the persistent snap-through dynamic is triggered in the absence of noise (Figure 8(b)). These results indicate that for the greater amplitude of harmonic base excitation, $\underline{a} = 5.85\,\mathrm{m/s^2}$, that induces the snap-through response in the absence of noise, the introduction of stochastic contributions to the excitation is adverse to DC power generation if the noise level is low because snap-through dynamics are inhibited, but additive noise may be a significant benefit to DC power delivery if the noise contribution is large enough, here around $\underline{\sigma}/\underline{a}\geq 2$. The theoretical predictions are in good agreement with the trend of DC power generation for increased noise when compared to the qualitative and quantitative results of simulation and experiment, as shown in Figure 7(b). This suggests that the new analytical model formulation and solution strategy

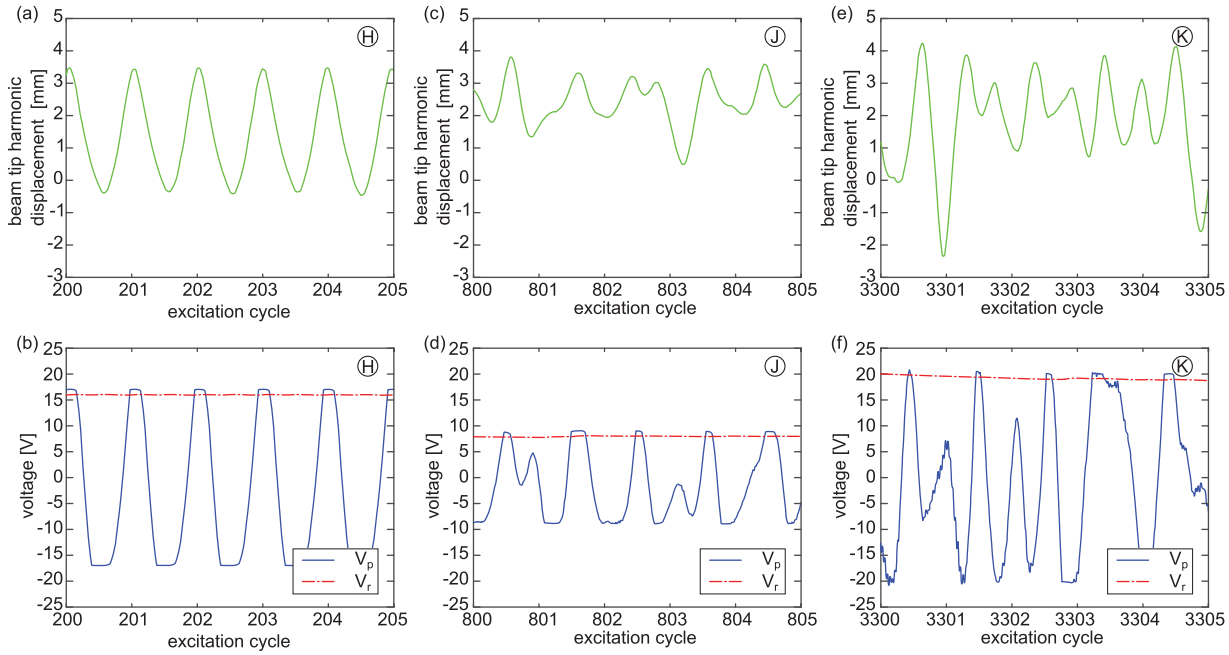

Figure 8. Portions of experimentally measured time series of points as indicated by labels H, J, and K from Figure 7(a). Here, (a, c, e) show beam tip displacement, and (b, d, f) show corresponding piezoelectric beam voltage and charging voltage across resistive load R = 470 kΩ.

may be used to assist implementation of nonlinear energy harvesters in practical application environments where the base acceleration available is neither purely harmonic nor purely stochastic.

Conclusion

In order to take advantage of the broadband and large power generation characteristics of nonlinear energy harvesters for self-sufficient sensors in structural health monitoring applications, this research investigated DC power generation from nonlinear vibration energy harvesters subjected to excitations that contain realistic combinations of harmonic and stochastic components. These efforts of this work established a new analytical method to predict the overall electromechanical responses induced under such excitations, including the DC power delivery from rectifier circuits coupled to such nonlinear harvester platforms. With numerical verification and experimentally validation, the accuracy of the analysis is exemplified. Through subsequent model and experimental studies, it is found that despite the introduction of stochastic excitation, the DC power may be increased from steady-state levels associated with the low amplitude intrawell dynamic regime. The noise excitation contribution has more intricate influences upon the snap-through responses: the additive noise reduces the mean DC power generation at low harmonic excitation frequencies when snap-through is achieved under pure harmonic excitations, while the stochastic excitations are beneficial when the ratio of noise standard deviation to harmonic amplitude is greater than about two. The outcomes indicate that the analytical model formulation and solution strategy have potential to assist in the design and implementation of nonlinear energy harvesters in real world application for improved, practical performance. In addition, due to the dependence of DC power generation on the resistive load, harmonic excitation characteristics, and additive stochastic excitation levels, optimization studies are promising directions for further investigations toward capitalizing on nonlinear energy harvesters deployed in real world environments.

Declaration of conflicting interests

The author(s) declared no potential conflicts of interest with respect to the research, authorship, and/or publication of this article.

Funding

The author(s) disclosed receipt of the following financial support for the research, authorship, and/or publication of this article: This research is supported by The Ohio State University Center for Automotive Research. The authors also acknowledge support from Midé Technology Corp.

References

Anh ND and Hieu NN (2012) The Duffing oscillator under combined periodic and random excitations. *Probabilistic Engineering Mechanics* 30: 27–36.

Anon (2015) *SG-Link-LXRS Wireless 2 Channel Analog Input Sensor Node* (user manual). Williston, VT: LORD Corporation.

Badel A and Lefeuvre E (2016) Nonlinear conditioning circuits for piezoelectric energy harvesters. In: Blokhina E, El Aroudi A, Alarcon E, et al. (eds) *Nonlinearity in Energy Harvesting Systems: Micro- and Nanoscale Applications*. Cham: Springer, pp. 321–359.

Baert K, Gyselinckx B, Torfs T, et al. (2006) Technologies for highly miniaturized autonomous sensor networks. *Microelectronics Journal* 37: 1563–1568.

Bulsara AR, Lindenburg K and Shuler KE (1982) Spectral analysis of a nonlinear oscillator driven by random and periodic forces. I. Linearized theory. *Journal of Statistical Physics* 27: 787–808.

Cottone F, Vocca H and Gammaitoni L (2009) Nonlinear energy harvesting. *Physical Review Letters* 102: 080601.

Daqaq MF (2011) Transduction of a bistable inductive generator driven by white and exponentially correlated Gaussian noise. *Journal of Sound and Vibration* 330: 2554–2564.

Elvin NG (2014) Equivalent electrical circuits for advanced energy harvesting. *Journal of Intelligent Material Systems and Structures* 25: 1715–1726.

Erturk A and Inman DJ (2011a) Broadband piezoelectric power generation on high-energy orbits of the bistable Duffing oscillator with electromechanical coupling. *Journal of Sound and Vibration* 330: 2339–2353.

Erturk A and Inman DJ (2011b) *Piezoelectric Energy Harvesting*. Chichester: John Wiley & Sons.

Erturk A, Hoffmann J and Inman DJ (2009) A piezomagnetoelastic structure for broadband vibration energy harvesting. *Applied Physics Letters* 94: 254102.

Feeny BF and Yuan CM (2001) Parametric identification of an experimental magneto-elastic oscillator. *Journal of Sound and Vibration* 247: 785–806.

Fosdick R, Ketema Y and Jang-Horng Y (1998) Vibration damping through the use of materials with memory. *International Journal of Solids and Structures* 35: 403–420.

Green PL, Papatheou E and Sims ND (2013) Energy harvesting from human motion and bridge vibrations: an evaluation of current nonlinear energy harvesting solutions. *Journal of Intelligent Material Systems and Structures* 24: 1494–1505.

Guyomar D, Badel A, Lefeuvre E, et al. (2005) Toward energy harvesting using active materials and conversion improvement by nonlinear processing. *IEEE Transactions on Ultrasonics, Ferroelectrics, and Frequency Control* 52: 584–595.

Harne RL and Dai Q (2017) Characterizing the robustness and susceptibility of steady-state dynamics in post-buckled structures to stochastic perturbations. *Journal of Sound and Vibration* 395: 258–271.

Harne RL and Wang KW (2014a) On the fundamental and superharmonic effects in bistable energy harvesting. *Journal of Intelligent Material Systems and Structures* 25: 937–950.

Harne RL and Wang KW (2014b) Prospects for nonlinear energy harvesting systems designed near the elastic stability limit when driven by colored noise. *Journal of Vibration and Acoustics* 136: 021009.

Harne RL and Wang KW (2017) *Harnessing Bistable Structural Dynamics: For Vibration Control, Energy Harvesting and Sensing*. Chichester: John Wiley & Sons.

Hikihara T and Kawagoshi T (1996) An experimental study on stabilization of unstable periodic motion in magneto-elastic chaos. *Physics Letters A* 211: 29–36.

Ibrahim RA (1985) *Parametric Random Vibration*. New York: John Wiley & Sons.

Ketema Y (1998) Averaging and bifurcations in an oscillator with a history dependent restoring force. *Journal of Sound and Vibration* 209: 187–198.

Leadenham S and Erturk A (2015) Nonlinear m-shaped broadband piezoelectric energy harvester for very low base accelerations: primary and secondary resonances. *Smart Materials and Structures* 24: 055021.

Lefeuvre E, Badel A and Richard C (2005) Piezoelectric energy harvesting device optimization by synchronous electric charge extraction. *Journal of Intelligent Material Systems and Structures* 16: 865–876.

Liang J and Liao WH (2012) Impedance modeling and analysis for piezoelectric energy harvesting systems. *IEEE/ASME Transactions on Mechatronics* 17: 1145–1157.

Mann BP and Sims ND (2009) Energy harvesting from the nonlinear oscillations of magnetic levitation. *Journal of Sound and Vibration* 319: 515–530.

Masana R and Daqaq MF (2011a) Electromechanical modeling and nonlinear analysis of axially loaded energy harvesters. *Journal of Vibration and Acoustics* 133: 011007.

Masana R and Daqaq MF (2011b) Relative performance of a vibratory energy harvester in mono- and bi-stable potentials. *Journal of Sound and Vibration* 330: 6036–6052.

Moon FC and Holmes PJ (1979) A magnetoelastic strange attractor. *Journal of Sound and Vibration* 65: 275–296.

Nayfeh AH and Serhan SJ (1990) Response statistics of nonlinear systems to combined deterministic and random excitations. *International Journal of Non-Linear Mechanics* 25: 493–509.

Panyam M, Masana R and Daqaq MF (2014) On approximating the effective bandwidth of bi-stable energy harvesters. *International Journal of Non-Linear Mechanics* 67: 153–163.

Pasharavesh A, Ahmadian MT and Zohoor H (2017) Coupled electromechanical analysis of MEMS-based energy harvesters integrated with nonlinear power extraction circuits. *Microsystem Technologies* 23: 2403–2420.

Priya S and Inman DJ (2009) *Energy Harvesting Technologies*. New York: Springer.

Randall RB (2011) *Vibration-based Condition Monitoring: Industrial, Aerospace and Automotive Applications*. Chichester: John Wiley & Sons.

Rao SS (2004) *Mechanical Vibrations*. 4th ed. Upper Saddle River, NJ: Pearson Prentice Hall.

Roberts JB and Spanos PD (1990) *Random Vibration and Statistical Linearization*. New York: John Wiley & Sons.

Roundy S, Wright PK and Rabaey J (2003) A study of low level vibrations as a power source for wireless sensor nodes. *Computer Communications* 26: 1131–1144.

Shu YC and Lien IC (2006a) Analysis of power output for piezoelectric energy harvesting systems. *Smart Materials and Structures* 15: 1499–1512.

Shu YC and Lien IC (2006b) Efficiency of energy conversion for a piezoelectric power harvesting system. *Journal of Micromechanics and Microengineering* 16: 2429–2438.

Shu YC, Lien IC and Wu WJ (2007) An improved analysis of the SSHI interface in piezoelectric energy harvesting. *Smart Materials and Structures* 16: 2253–2264.

Sodano HA, Inman DJ and Park G (2005) Comparison of piezoelectric energy harvesting devices for recharging batteries. *Journal of Intelligent Material Systems and Structures* 16: 799–807.

Soong TT (2004) *Fundamentals of Probability and Statistics for Engineers*. Chichester: John Wiley & Sons.

Stanton SC, McGehee CC and Mann BP (2010) Nonlinear dynamics for broadband energy harvesting: investigation of a bistable piezoelectric inertial generator. *Physica D* 239: 640–653.

Stanton SC, Owens BAM and Mann BP (2012) Harmonic balance analysis of the bistable piezoelectric inertial generator. *Journal of Sound and Vibration* 331: 3617–3627.

Tang L, Yang Y and Soh CK (2010) Toward broadband vibration-based energy harvesting. *Journal of Intelligent Material Systems and Structures* 21: 1867–1897.

Turner JD and Pretlove AJ (1988) A study of the spectrum of traffic-induced bridge vibration. *Journal of Sound and Vibration* 122: 31–42.

Virgin LN (2000) *Introduction to Experimental Nonlinear Dynamics*. Cambridge: Cambridge University Press.

Wu Y, Badel A, Formosa F, et al. (2012) Piezoelectric vibration energy harvesting by optimized synchronous electric charge extraction. *Journal of Intelligent Material Systems and Structures* 24: 1445–1458.

Zuo L and Zhang PS (2013) Energy harvesting, ride comfort, and road handling of regenerative vehicle suspensions. *Journal of Vibration and Acoustics* 135: 011002.